Pergamon

0043-1354(95)00253-7

Wat. Res. Vol. 30, No. 5, pp. 1049–1056, 1996

0043-1354/96 $15.00 + 0.00

SHEAR-INDUCED FLOCCULATION: THE EVOLUTION OF FLOC STRUCTURE AND THE SHAPE OF THE SIZE DISTRIBUTION AT STEADY STATE

PATRICK T. SPICER and SOTIRIS E. PRATSINIS*

Department of Chemical Engineering, ML 171, University of Cincinnati, Cincinnati, OH 45221-0171, U.S.A.

(First received June 1995; accepted in revised form October 1995)

Abstract—The flocculation of polystyrene particles in a stirred tank was studied at various shear rates (63–129 s^{-1}) and aluminum sulfate, $Al_2(SO_4)_3\ 16H_2O$, flocculant concentrations. The competition between coagulation and fragmentation during shear-induced flocculation determined the equilibrium or steady state particle (floc) structure and size distribution. The evolution of the floc structure with time was monitored by image analysis of digitized floc images. The average floc structure became less open or irregular as the floc size distribution attained steady state as a result of shear-induced breakage/restructuring. At high alum (flocculant) concentrations, the steady state floc size distribution appeared to be self-preserving with respect to shear rate. In contrast, at lower flocculant concentrations, the steady state floc size distribution narrowed with increasing shear rate as the large tail of the distribution was pushed to smaller particle sizes by shear-induced fragmentation. Copyright © 1996 Elsevier Science Ltd.

Key words—self-similarity, shear-induced flocculation, aluminum sulfate, particle size distributions, floc structure, fractal

INTRODUCTION

The removal of particles from a liquid suspension is one of the basic types of separations in both drinking water and waste water treatment. The particles are frequently in the micron or sub-micron size range and are difficult to remove by conventional means like sedimentation or filtration. Flocculation is often used to increase the average particle (floc) size and enhance solids removal.

Several phases of floc growth occur during flocculation. Initially, particle (floc) growth is dominant, particles combine by coagulation and their size increases rapidly. As flocculation continues, the flocs form large, porous and open structures that are more susceptible to fragmentation by fluid shear (Tambo, 1991). As a result, the final floc size distribution is the balance (steady state) between particle growth and breakage (Reich and Vold, 1959; Parker *et al.*, 1972; Lu and Spielman, 1985; Oles, 1992; Spicer, 1995). Furthermore, the floc structure is important since it determines floc size and density and, thus, will influence the solids removal efficiency during sedimentation. The structure of the flocs at steady state also depends on the process conditions. Virtually no experimental studies of the dynamic evolution of the floc structure have been performed. Most studies have focused on the determination of floc structure at steady state or on samples collected at a constant residence time (i.e. Klimpel and Hogg, 1986; Sonntag and Russel, 1986; Li and Ganczarczyk, 1990; Clark and Flora, 1991; Jiang and Logan, 1991; Logan and Kilps, 1995).

Reich and Vold (1959) studied the effect of shear rate on a suspension of ferric hydroxide and found that the final average floc size was the result of a steady state between breakage and growth. Tambo and Watanabe (1979a) theoretically and experimentally studied the turbulent flocculation of kaolin using aluminum sulfate as a flocculant. They found that the steady state distribution of sedimentation rates for the suspension collapsed onto a single curve when normalized by two variables. They inferred that the steady state floc size distribution was self-preserving but did not offer direct experimental proof. More recently, Oles (1992) monitored the average floc size at steady state as a function of shear rate for coagulation of polystyrene particles using NaCl as a destabilizer (flocculant). He observed a rapid initial floc growth rate that slowed as floc breakage began to occur. A leveling off of the floc sizes at steady state was observed and attributed to an equilibrium between floc growth and breakage. Increasing the amount of floc breakage increased the floc density but decreased the average floc size (Oles, 1992).

This paper addresses the attainment of steady state by a flocculating suspension as a function of process conditions. Emphasis is placed on the evolution of

*Author to whom all correspondence should be addressed.

the floc structure and the properties of the steady state floc size distribution. Measurements of floc size by image analysis are used to evaluate the development of the steady state floc structure and the form of the steady state size distribution. Conditions that lead to asymptotic or self-preserving steady state size distributions with respect to shear rate and flocculant concentration are identified. This is particularly useful in understanding the degree of control that can be exerted over floc formation.

EXPERIMENTAL

Apparatus and materials

All experiments were conducted in a closed, 2.8 l, baffled, stirred tank of standard configuration (Holland and Chapman, 1966) using a six-blade, disk-mounted (Rushton) impeller. Figure 1 shows the relative dimensions of the employed impeller-tank. The turbulent shear rate within the stirred tank was characterized by the average velocity gradient or shear rate, G (Camp and Stein, 1943)

$$G = \left(\frac{\epsilon}{\nu}\right)^{\frac{1}{2}} \tag{1}$$

where ν is the kinematic viscosity of the suspending fluid (here, water) and ϵ is the average turbulent energy dissipation rate (Godfrey *et al.*, 1989)

$$\epsilon = \left(\frac{P_0 N^3 D^5}{V}\right) \tag{2}$$

where P_0 is the impeller power number, N is the impeller speed, V is the stirred tank volume, and D is the impeller diameter. The P_0 is obtained using the standard power curve for the employed six-blade impeller (p. 78, Fig.4-4 in Holland and Chapman, 1966). Although the flow conditions within a stirred tank are non-homogeneous (Cutter, 1966; Sprow, 1967; Konno *et al.*, 1983), Equations 1 and 2 are used to provide a basis for comparison with previous work. The impeller rotational velocity was measured with an optical tachometer (Ono Sokki HT-4100). The Kolmogorov microscale, η, characterizing the length scale of the energy dissipating turbulent eddies is (Spielman, 1978)

$$\eta = \left(\frac{\nu^3}{\epsilon}\right)^{\frac{1}{4}}. \tag{3}$$

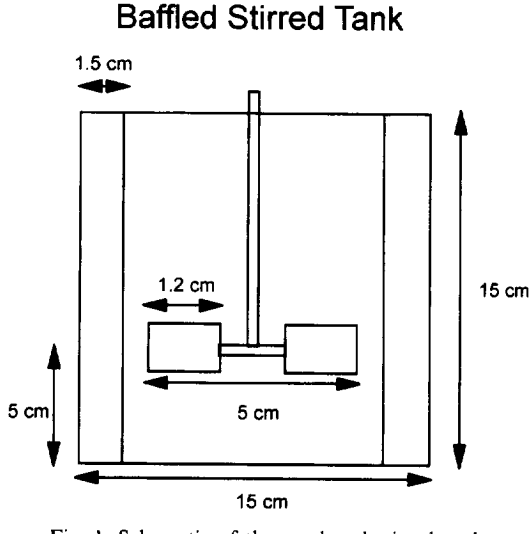

Fig. 1. Schematic of the employed stirred tank.

Monodisperse, spherical, polystyrene particles with a diameter of 0.87 μm (by Transmission Electron Microscopy) and a density of 1.05 g/cm^3 were flocculated in distilled water (that had been buffered with $NaHCO_3$) at solids volume fractions of $\phi = 8.3 \times 10^{-5}$ and 2.1×10^{-5}. Polystyrene is an idealized model particle because of its low density and spherical shape. The polystyrene particles had been prepared using the method of De Boer (1987) and concentrated by vacuum evaporation to minimize the volume injected into the stirred tank suspension. The flocculant was aluminum sulfate hydrate or alum, $Al_2(SO_4)_3$ $16H_2O$ (Aldrich, 98%). The suspension was buffered with sodium hydrogen carbonate ($NaHCO_3$) (Aldrich, 99%) at a concentration of 1 mM and the pH was maintained at 7 ± 0.2 by the addition of 0.1 N HCl or NaOH in all experiments.

Procedure and measurements

A small volume (1–2 cm^3) of the polystyrene suspension was injected into the water volume in the stirred tank and mixed before flocculation was initiated. The particles were suspended and stirred for 5 min at a high shear rate, $G = 540$ s^{-1} (500 r.p.m.), to break up any initially present agglomerates. This procedure was checked using a control experiment in which no flocculant was added and the individual primary particles were observed to be stable and remain un-flocculated. Using a hypodermic needle, a measured dose of the acidic stock flocculant solution (2 g alum per liter) was then added at the tip of the impeller and mixed with the suspension for 1 min at $G = 540$ s^{-1}. The flocculant dose was expressed as total milligrams of $Al_2(SO_4)_3$ $16H_2O$ per liter of suspension. Following the rapid mixing, flocculation was then carried out at a constant shear rate. A 1 cm^3 sample was withdrawn periodically for image analysis. This sample volume was found sufficient to provide reproducible size distribution measurements. A minimum of 500 particles were counted during the determination of each size distribution. Microscopic analysis was carried out using an optical microscope (Nikon, Labophot) connected to a CCTV camera (Hitachi-Denshi).

Samples were taken by inserting the wide end of a 0.5 cm i.d. pipette (Gibbs and Konwar, 1982) below the suspension surface, covering the end, and withdrawing carefully. The image analysis of the flocs was carried out by placing a drop on a flat microscope slide without a cover slip and videotaping the corresponding image. The video was then digitized and analyzed with Global Lab Image v. 2.0 software.

The resolution of the microscope defines the lower detection limit of the image analysis technique. Under 400X magnification a 1 μm floc appears to be 0.4 mm in length. The lower detection limit of the image analysis software, however, is only about 1 mm ($\sim$2.5 μm floc at 400X). At 100X and 40X magnifications, the lower detection limits were 10 and 25 μm, respectively. To minimize the influence of the lower detection limit, image analysis data were used only when more than 95% by count (or greater) of the visually observed particles could be resolved by the image analysis software. The maximum length (size), perimeter, and cross sectional area of the flocs were obtained by image analysis, as the viewed flocs had settled to their most stable configuration. The image analysis software identifies an area of the image as a particle if the grey values of the contiguous pixels exceed a user defined threshold value. Before analysis the software was calibrated using a slide marked at known intervals. An image of the slide was digitized and the number of pixels between two marks corresponding to 10 μm was recorded on the screen.

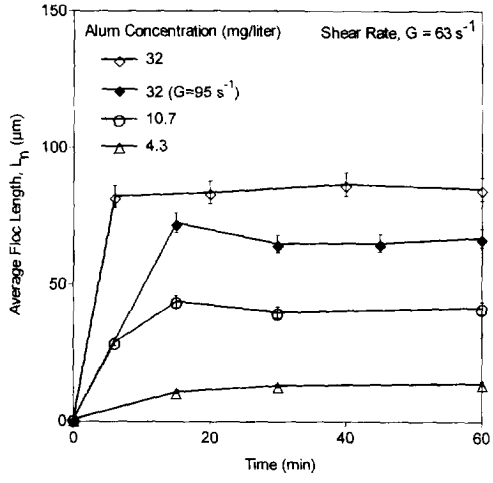

Fig. 2. Evolution of the average floc length, L_n, as a function of time for the flocculation of polystyrene at various alum concentrations ($c = 4.3$–32 mg/l) and $G = 63$ s^{-1} (open symbols) and $G = 95$ s^{-1} (solid diamonds). After attainment of steady state, L_n no longer changes with time.

RESULTS AND DISCUSSION

The attainment of steady state

Floc size distributions were obtained by image analysis of videotaped, digitized images of the suspension samples. All data points represent the results of 2–3 replicate experiments with a reproducibility error less than 5%. The employed alum concentrations were chosen to represent the three classical regimes of particle destabilization, adsorption destabilization: 4.3 mg/l; sweep flocculation: 32 mg/l; and the intermediate regime: 10.7 mg/l (Amirtharajah and Mills, 1982). These concentrations are near the low end (10–100 mg/l) of practical applications of flocculation (Amirtharajah and Mills, 1982) but also allow comparison with the trends predicted by the precipitation-charge neutralization theory (Dentel and Gossett, 1988). All subsequent discussion of alum destabilization effects is based on this theory.

The employed shear rates (63, 95, 129 s^{-1}; 116, 152, 184 r.p.m.) were chosen to eliminate the possibility of significant sedimentation of the larger flocs. Although the G values are relatively high when compared to those of a practical flocculation system (10–40 s^{-1}), they allow the observation of both particle coagulation and fragmentation phenomena that are responsible for the attainment of the steady state size distribution.

A suspension was considered to have attained steady state when the floc size distribution no longer changed with time. Figure 2 shows the evolution of the arithmetic (number) average floc length, L_n, at $G = 63$ s^{-1} (open symbols) for three alum concentrations. Depending on the alum concentration, after some time [about 25 min for $G = 63$ s^{-1} and $c = 10.7$ mg/l alum (Fig. 2)] the floc size distribution remains constant and has reached steady state. Increased alum concentration produces stronger and larger flocs and results in a faster attainment of steady state. Furthermore, increasing the shear rate (Fig. 2: solid diamonds) decreases the steady state floc size as a result of increased floc breakage.

Figure 3 summarizes the average steady state floc length, $L_{n\infty}$ obtained by image analysis as a function of shear rate ($G = 63$, 95, 129 s^{-1}) and alum concentration ($c = 4.3$, 10.7, and 32 mg/l). The data of Oles (1992) are also shown for the shear-induced flocculation of 2.17 μm polystyrene particles with NaCl at $\phi = 10^{-5}$. The $L_{n\infty}$ depends on the relative significance of shear-induced growth and breakage, each of which is in turn a function of the applied shear rate and alum concentration. In Fig. 3, increasing shear increases the rate of floc breakage, resulting in a smaller average floc size at steady state. At the early stages of flocculation, shear increases particle collisions and growth. As the particles grow, breakage becomes more significant as the size range of flocs susceptible to breakage by turbulent eddies increases (Kusters, 1991). This is consistent with Parker *et al.* (1972), Tambo and Watanabe (1979a), and Oles (1992) who observed that the average floc size decreased with increasing shear rate.

Figure 3 also shows the Kolmogorov microscale of turbulence, η, for the employed range of shear rates. The variation of η with G follows the variation of $L_{n\infty}$ with shear for $c = 32$ mg/l and 10.7 mg/l as well as the data of Oles (1992). Recalling that the smallest eddy size is of the order of η, we observe that the shear field determines the size characteristics of the resulting flocs at high flocculant concentrations.

The increasing L_n with alum concentration clearly indicates the strengthening of the linkage between the

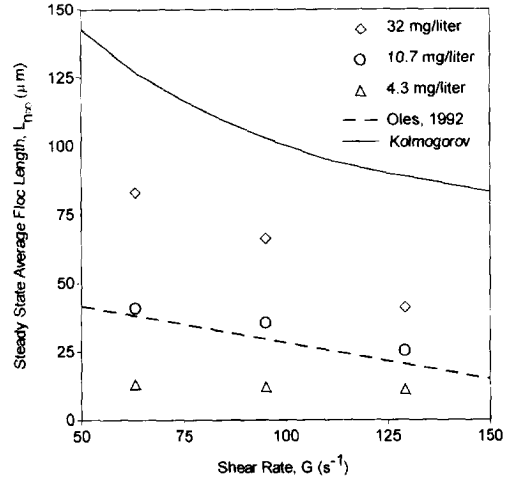

Fig. 3. The average steady state floc length, $L_{n\infty}$, as a function of shear rate and alum concentration. Also plotted are the flocculation results of Oles (1992) and the calculated values of the Kolmogorov microscale, η. The data of Oles (1992) are in good agreement with the results of this study. The variation of η and $L_{n\infty}$ with G are in good agreement.

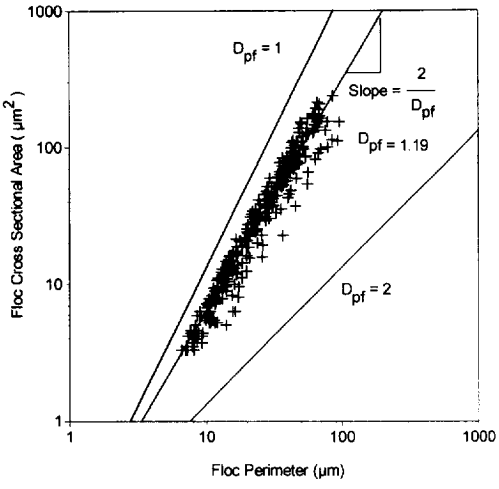

Fig. 4. Determination of the fractal dimension, D_{pf}, from image analysis measurements of floc cross-sectional area and perimeter at $\phi = 2.1 \times 10^{-5}$. The two limiting cases of D_{pf} are also shown for comparison of the relative floc structure.

primary particles of the floc. Depending on the mode of destabilization (Dentel and Gossett, 1988), increasing the flocculant concentration will either increase the average particle size or the particle number concentration. Either result will increase the floc growth rate unless restabilization by charge reversal occurs (Dentel and Gossett, 1988). Increased alum concentration increases the floc growth rate and strength of the linkage between the primary particles in the floc (by increasing the $Al(OH)_3$ surface coverage), making it more resistant to breakage. As a result, the floc size at steady state increases with increasing alum concentration. This is in agreement with Francois (1988) who found an increase in both the floc growth rate and the collision efficiency with increased alum concentration during kaolin flocculation.

The evolution of floc structure

The concepts of fractal geometry (Mandelbrot, 1983) provide a mathematical framework for description of the structure of irregular flocs. A characteristic dimension of the floc, in this case the perimeter (P), can be related to the projected area of the floc (A) by (Mandelbrot *et al.*, 1984)

$$A \propto P^{\frac{2}{D_{pf}}} \tag{4}$$

where D_{pf} is the perimeter-based fractal dimension of the floc. This equation was used by Li and Ganczarczyk (1991) to characterize very thin slices of activated sludge flocs.

Provided that there are several primary particles in each floc, the average perimeter-based fractal dimension, D_{pf}, of the flocs can be estimated from Equation 4 using a log–log plot of the floc perimeter and cross sectional area (Fig. 4). The D_{pf} is related to the floc surface morphology since D_{pf} varies between 2 (a line) and 1 (the projected area of a solid sphere, a circle). Large values of D_{pf} therefore represent open and irregular floc structures. Figure 4 shows these limiting cases as well as the data obtained after 120 min of flocculation at $G = 63\ s^{-1}$ and $c = 2.1$ mg/l. For this case, regression analysis gives $D_{pf} = 1.19$.

Figure 5 shows the evolution of D_{pf} and the corresponding L_n at these conditions. The various velocity gradients within a stirred tank produce a distribution of floc structures as a result of simultaneous shear-induced growth, breakage, and restructuring. The error bars in Fig. 5 indicate the range of D_{pf} values in the sample. These values were determined from the standard error (95% confidence interval) of the slope fit to the area vs perimeter data. Figure 5 shows that D_{pf} increases from its initial value ($D_{pf} = 1$) and reaches a maximum value of $D_{pf} = 1.29$ as the flocs grow and become more porous. When breakage begins to dominate, D_{pf} decreases slightly until it reaches a steady state value of about $D_{pf} = 1.19$. This is in agreement with Tambo and Watanabe (1979a) and Oles (1992) who suggested that a decreased floc porosity (as indicated here by the decreasing fractal dimension) results from the production of strong, dense fragments by preferential breakage of the flocs at weak points. Li and Ganczarczyk (1991) reported $D_{pf} = 1.13$–1.22 for activated sludge flocs. In Fig. 5, the spread of the D_{pf} narrows as the floc size reaches steady state. This may result from restructuring and/or compaction of the flocs by shear forces (Jullien and Meakin, 1989). Francois (1987) observed a similar compaction of flocs at extended flocculation times.

Figure 6 shows the measured steady state perimeter-based fractal dimension, $D_{pf\infty}$ at all employed alum concentrations and shear rates. Error bars represent the variation of the measured value of

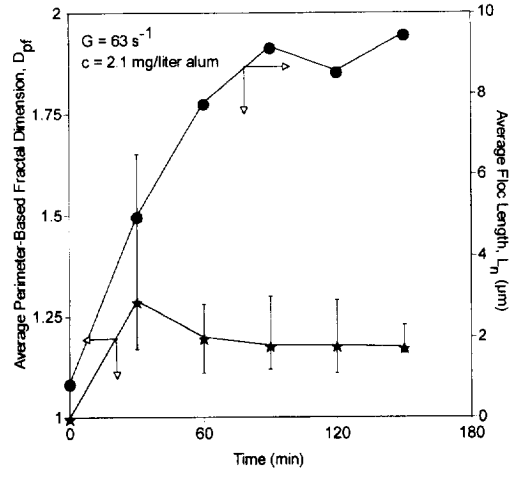

Fig. 5. Evolution of the L_n and fractal dimension, D_{pf}, for $G = 63\ s^{-1}$ and $c = 2.1$ mg/l at $\phi = 2.1 \times 10^{-5}$. After sufficiently long times, both L_n and D_{pf} approach an asymptotic, steady state value.

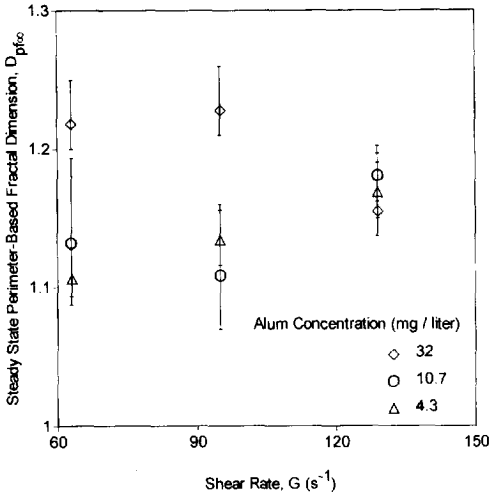

Fig. 6. The steady state fractal dimension, $D_{pf\infty}$, as a function of shear rate at three alum concentrations at $\phi = 8.3 \times 10^{-5}$. Increased alum concentration produces more open floc structures at constant shear rate. The effect of increasing shear is more dramatic at high alum concentrations.

$D_{pf\infty}$ between replicate experiments. The $D_{pf\infty}$ was not affected significantly by flocculant concentration at the two lower alum concentrations (10.7 and 4.3 mg/l) at all shear rates. However, at a high alum concentration, $c = 32$ mg/l, the $D_{pf\infty}$ was larger (indicating more open structures) than at the two lower alum concentrations. At higher alum concentrations and rather low shear rates, the increased linkage strength within the floc structure may increase resistance to breakage or restructuring resulting in more open floc structures at steady state. This is consistent with Tambo and Watanabe (1979a) who found increasingly open floc structures as the ratio of alum concentration to suspended solids was increased.

Increasing, however, the shear rate ($G = 129$ s^{-1}) at high flocculant concentrations, ($c = 32$ mg/l) decreased the $D_{pf\infty}$ (Fig. 6). As the shear rate increases, the increased amount of breakage/regrowth and restructuring produces more compact floc structures (Tambo and Watanabe, 1979b). At high shear rates, there is virtually no difference in the floc structure regardless of flocculant conditions.

Effect of process variables on the steady state floc size distribution

The effect of shear rate on the steady state floc size (length) distribution is shown in Fig. 7(a) at $c = 32$ mg/l and $\phi = 8.3 \times 10^{-5}$. Clearly, increasing shear reduces the large tail of the distribution and decreases the overall floc size, shifting the entire size distribution into the smaller sizes. When, however, the floc length, L, is scaled with its average, L_n, all data collapse onto a single curve [Fig. 7(b)]!

Some scatter is observed in the lower size ranges that may be attributed to the lower size limit of the image analyzer. At these conditions, shear has no effect on the shape of the normalized steady state size distribution, making it self-preserving with respect to shear. The self-preserving nature of the steady state floc size distribution simplifies floc size characterization. If the steady state size distribution of a flocculating suspension is self-preserving, one needs only to estimate one variable of the distribution, e.g. the average diameter, and then the entire distribution can be obtained.

Figure 8 shows (a) the dimensional and (b) the normalized steady state floc length distributions obtained at an alum concentration of 10.7 mg/l. As in Fig. 7(a), the steady state distributions in Fig. 8(a) narrow with increasing shear as fragmentation increases. Upon normalization, these distributions do not collapse onto a single line as in Fig. 7(b) but as the shear rate increases they become narrower

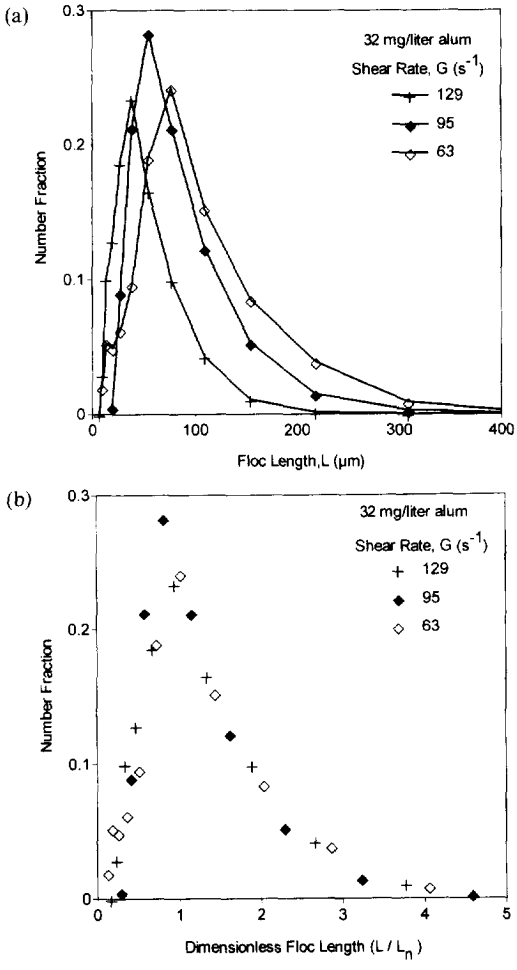

Fig. 7. (a) Steady state floc length distributions as a function of shear rate for an alum concentration of 32 mg/l at $\phi = 8.3 \times 10^{-5}$ ($N_T = 2774$ at $G = 129$ s^{-1}, 6573 at 95 s^{-1}, 3181 at 63 s^{-1}). Increased shear narrows the floc size distribution by decreasing the overall floc size. (b) Normalized form of the steady state floc length distribution. The curves collapse onto a single line and are self-similar with respect to shear.

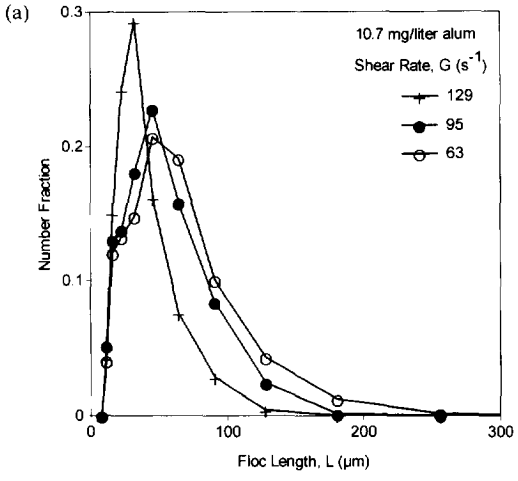

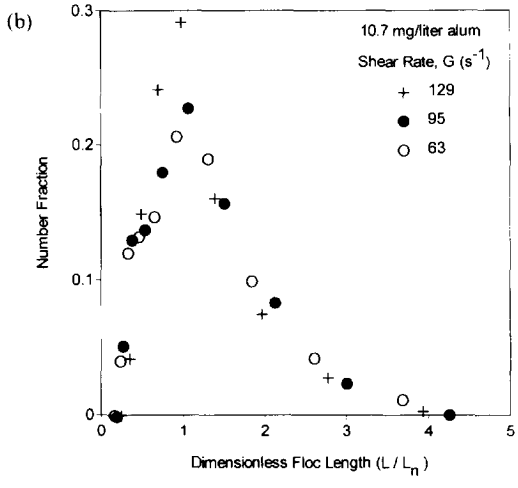

Fig. 8. (a) Steady state floc length distributions as a function of shear rate for an alum concentration of 10.7 mg/l at $\phi = 8.3 \times 10^{-5}$ ($N_T = 2813$ at $G = 129$ s^{-1}, 1820 at 95 s^{-1}, 3215 at 63 s^{-1}). (b) Normalized form of the steady state distribution. Decreasing alum concentration increases the effect of shear-induced breakage on the floc size distribution and increases the deviation from self-similarity by narrowing the normalized size distribution.

[Fig. 8(b)]. This effect is most pronounced at the lowest alum concentration, 4.3 mg/l [Fig. 9(a) and (b)] where the linkage between primary particles is the weakest. In Fig. 9(a), increasing shear-induced fragmentation produces a second mode at the smallest floc sizes. The normalized form of these distributions deviates from self-similarity as a result of the dramatic shear effects [Fig. 9(b)].

The geometric standard deviation at steady state, $\sigma_{g\infty}$, for each of the floc size distributions in Fig. 7(a), Fig. 8(a), and Fig. 9(a) is shown in Fig. 10 as a function of shear rate for all three alum concentrations. The bars indicate the variation of the measured $\sigma_{g\infty}$ for replicate experiments. The σ_g was calculated using (Hinds, 1982)

$$\sigma_g = \exp\left[\frac{\Sigma n_i(\ln L_i - \ln L_g)^2}{N_T - 1}\right]^{\frac{1}{2}} \quad (5)$$

where N_T is the total number of flocs in the distribution and L_g is the geometric average floc (maximum) length (Hinds, 1982)

$$L_g = \exp\left[\frac{\Sigma n_i \ln L_i}{N_T}\right]. \quad (6)$$

The σ_g indicates the width of the size distribution, where $\sigma_g = 1$ corresponds to a monodisperse distribution while increasing $\sigma_g > 1$ indicates increasingly broad distributions. At the two lower alum concentrations (4.3 and 10.7 mg/l), increasing shear rate narrows the size distribution by trimming the large tail of the floc size distribution while the small tail remains virtually unchanged as the smallest

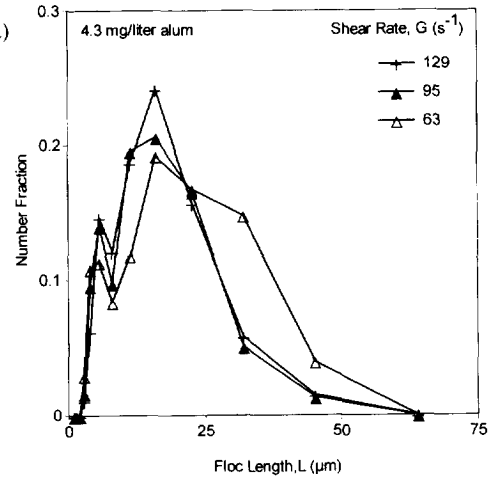

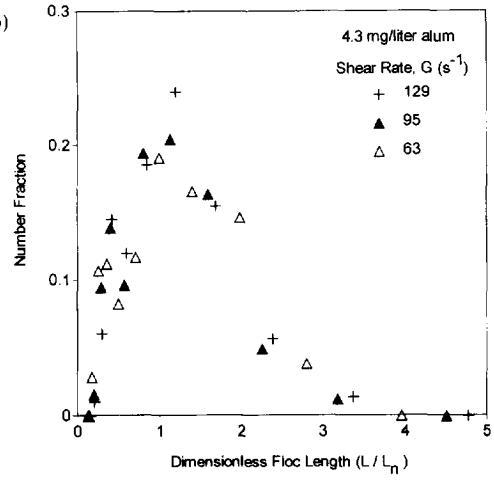

Fig. 9. (a) Steady state floc length distributions as a function of shear rate for an alum concentration of 4.3 mg/l at $\phi = 8.3 \times 10^{-5}$ ($N_T = 503$ at $G = 129$ s^{-1}, 592 at 95 s^{-1}, 791 at 63 s^{-1}). (b) Increased floc breakage at this low alum concentration results in the formation of a second mode in the distribution.

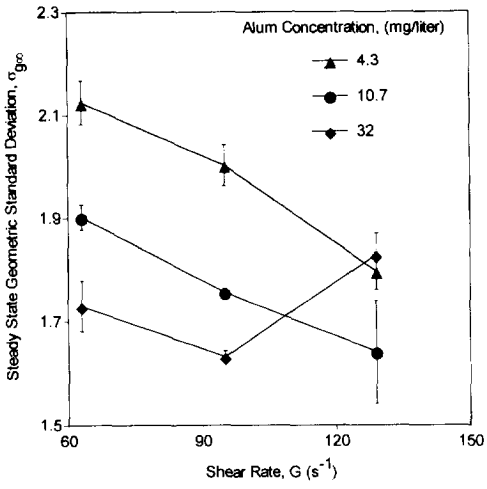

Fig. 10. Geometric standard deviation, $\sigma_{g\infty}$, of the steady state floc size distributions as a function of alum concentration and shear rate. The value of $\sigma_{g\infty}$ decreases with increasing shear rate as fragmentation becomes more dominant. Increasing alum concentration at a constant shear rate also decreases the value of $\sigma_{g\infty}$. At high alum concentrations, the $\sigma_{g\infty}$ remains essentially constant ($\sigma_{g\infty} \approx 1.7$) within experimental variation.

particle size is that of the primary particle. Higher shear rates mostly reduce the upper end of the distribution, resulting in a narrower overall distribution. The $\sigma_{g\infty}$ also decreases with increasing alum concentration. At the highest alum concentration, for which the size distributions display self-similarity, the $\sigma_{g\infty}$ shows no trend with shear and remains constant. Self-similarity is apparently exhibited only at excess flocculant concentrations, probably as a result of the effects of the larger amount of $Al(OH)_3$ precipitate present (increased resistance to breakage and increased floc growth rate).

The steady state floc size distribution is the result of the balance between coagulation and fragmentation. The relative strength of each phenomenon determines the evolution and specific value of the steady state floc size distribution. At low alum concentrations, the linkage between the primary particles in the floc is weak and the flocs are more likely to break. As a result, fragmentation greatly affects the large tail of the distribution and prevents the advancement of the floc size distribution from the lower size range. By increasing the alum concentration, the floc strength is increased, so shear-induced coagulation and fragmentation balance each other far away from the initial particle size. The resulting steady state floc size distribution is fully developed and becomes self-preserving with respect to shear.

CONCLUSIONS

An experimental study of the effect of shear rate and flocculant concentration during flocculation of polystyrene particles was carried out. After sufficiently long times, the floc size distribution reached an equilibrium or steady state size distribution from the competition between coagulation and fragmentation. Increased shear decreased the average steady state floc size as determined by image analysis. Increasing the flocculant concentration increased the floc growth rate and the steady state floc size while increased shear always reduced floc size at steady state.

The dynamic evolution of floc structure was monitored by image analysis of digitized floc images. The perimeter-based fractal dimension, D_{pf}, of the flocs was found to initially increase (more open structure) and then slightly decrease (more compact structure) and reach a steady state as a result of shear-induced breakage and/or restructuring. Shear-induced restructuring also narrowed the range of floc structures as steady state was attained.

The normalized steady state floc size distributions appear to be self-similar with respect to shear at high flocculant concentrations where the floc size distribution is fully developed. At lower flocculant concentrations, increasing fluid shear appeared to narrow the steady state floc size distributions as increased floc breakage limited floc growth and narrowed the floc size distribution.

Acknowledgements—We wish to acknowledge Doug Bowling and the Materials Science Department of the University of Cincinnati for providing access to the image analysis equipment. We acknowledge stimulating discussions with Dr Karl Kusters (currently with Shell Oil Co.) at the early stages of this project. Support by the National Science Foundation, Grant CTS-8957042, is gratefully acknowledged. We thank the journal referees for helpful suggestions during the review of the manuscript.

REFERENCES

Amirtharajah A. and Mills K. M. (1982) Rapid-mix design for mechanisms of alum coagulation. *J. Am. Wat. Wks Assoc.* **74,** 210–216.

Camp T. R. and Stein P. G. (1943) Velocity gradients and internal work in fluid motion. *J. Boston Soc. Civ. Engrs* **30,** 219.

Clark M. M. and Flora J. R. V. (1991) Floc restructuring in varied turbulent mixing. *J. Coll. Int. Sci.* **147,** 407–421.

Cutter L. A. (1966) Flow and turbulence in a stirred tank. *A.I.Ch.E.J.* **12,** 35–45.

de Boer G. B. J. (1987) Coagulation in stirred tanks. Ph. D. thesis, Eindhoven Univ. of Technology, The Netherlands.

Dentel S. K. and Gossett J. M. (1988) Mechanisms of coagulation with aluminum salts. *J. Am. Wat. Wks Assoc.* **80,** 187–198.

Francois R. J. (1987) Ageing of aluminum hydroxide flocs. *Wat. Res.* **21,** 523–531.

Francois R. J. (1988) Growth kinetics of hydroxide flocs. *J. Am. Wat. Wks Assoc.* **80,** 92–96.

Gibbs R. J. and Konwar L. N. (1982) Effect of pipetting on mineral flocs. *Environ. Sci. Technol.* **16,** 119–121.

Godfrey J. C., Obi F. I. N. and Reeve R. N. (1989) Measuring drop size in continuous liquid–liquid mixers. *Chem. Engng Prog.* **85,** 61–69.

Hinds W. C. (1982) *Aerosol Technology*, p. 85. Wiley-Interscience, New York.

Holland F. A. and Chapman F. S. (1966) *Liquid Mixing and Processing in Stirred Tanks*. Reinhold, London.

Jiang and Logan B. E. (1991) Fractal dimensions of aggregates determined from steady state size distributions. *Environ. Sci. Technol.* **25,** 2031–2038.

Jullien R. and Meakin P. (1989) Simple models for the restructuring of three-dimensional ballistic aggregates. *J. Coll. Int. Sci.* **127,** 265–272.

Klimpel R. C. and Hogg R. (1986) Effects of flocculation conditions on agglomerate structure. *J. Coll. Int. Sci.* **113,** 121–131.

Konno M., Aoki M. and Saito S. (1983) Scale effect on breakup process in liquid–liquid agitated tanks. *J. Chem. engng Japan* **16,** 312–317.

Kusters K. A. (1991) The influence of turbulence on aggregation of small particles in agitated vessels. Ph. D. thesis, Eindhoven Univ. of Technology, The Netherlands.

Li D. and Ganczarczyk J. J. (1990) Structure of activated sludge flocs. *Biotechnol. Bioengng* **35,** 57.

Li D. and Ganczarczyk J. J. (1991) Size distribution of activated sludge flocs. *Res. J. Wat. Pollut. Control. Fed.* **63,** 806–814.

Logan B. E. and Kilps J. R. (1995) Fractal dimensions of aggregates formed in different fluid mechanical environments. *Wat. Res.* **21,** 443–453.

Lu C. F. and Spielman L. A. (1985) Kinetics of floc breakage and aggregation in agitated liquid suspensions. *J. Coll. Int. Sci.* **103,** 95–105.

Mandelbrot B. B. (1983) *The Fractal Geometry of Nature*. W. H. Freeman, San Francisco, Calif.

Mandelbrot B. B., Passoja D. E. and Paullay A. J. (1984) Fractal character of fracture surfaces of metals. *Nature* **308,** 721–722.

Meakin P. (1988) Fractal aggregates. *Adv. Coll. Int. Sci.* **28,** 249–331.

Oles V. (1992) Shear-induced aggregation and breakup of polystyrene latex particles. *J. Coll. Int. Sci.* **154,** 351–358.

Pandya J. D. and Spielman L. A. (1982) Floc breakage in agitated suspensions: theory and data processing strategy. *J. Coll. Int. Sci.* **90,** 517–531.

Pandya J. D. and Spielman L. A. (1983) Floc breakage in agitated suspensions: effect of agitation rate. *Chem. Engng Sci.* **18,** 1983–1992.

Parker D. S., Kaufman W. J. and Jenkins D. (1972) Floc breakup in turbulent flocculation processes. *J. San. engng Div., Proc. ASCE* **98,** 79–99.

Reich I. and Vold R. D. (1959) Flocculation-deflocculation in agitated suspensions. I. Carbon and ferric oxide in water. *J. Phys. Chem.* **63,** 1497–1501.

Sonntag R. C. and Russel W. B. (1986) Structure and breakup of flocs subjected to fluid stresses I. Shear experiments. *J. Coll. Int. Sci.* **113,** 399–413.

Spicer P. T. (1995) The dynamics of shear-induced flocculation in a stirred tank. M.S. thesis, Univ. of Cincinnati, Ohio.

Spielman L. A. (1978) Hydrodynamic aspects of flocculation. In *The Scientific Basis of Flocculation* (Edited by Ives K. J.). Sijthoff & Noordhoff, The Netherlands.

Sprow F. B. (1967) Drop size distributions in strongly coalescing agitated liquid–liquid systems. *A.I.Ch.E. J.* **13,** 995–998.

Tambo N. (1991) Basic concepts and innovative turn of coagulation/flocculation. *Wat. Supply* **9,** 1–10.

Tambo N. and Watanabe Y. (1979a) Physical aspect of flocculation process—1. Fundamental treatise. *Wat. Res.* **13,** 429–439.

Tambo N. and Watanabe Y. (1979b) Physical characteristic of flocs: I. The floc density function and aluminum floc. *Wat. Res.* **13,** 409–419.